Available online at www.sciencedirect.com
ScienceDirect
Journal of Magnesium and Alloys 8 (2020) 989–998
www.elsevier.com/locate/jma

Review

Review of Mg alloy corrosion rates

Andrej Atrens[a,*], Zhiming Shi[a], Syeda U. Mehreen[a], Sean Johnston[a], Guang-Ling Song[b], Xianhua Chen[c,d], Fusheng Pan[c,d]

[a] The University of Queensland, School of Mechanical and Mining Engineering, Centre for Advanced Materials Processing and Manufacturing (AMPAM), St Lucia, Qld 4072, Australia
[b] Xiamen University, College of Materials, Center for Marine Materials Corrosion & Protection, State Key Laboratory of Physical Chemistry of Solid Surfaces, 422 Siming Rd., Xiamen 361005, China
[c] Chongqing University, College of Materials Science and Engineering, Chongqing, 400045, China
[d] Chongqing University, National Engineering Research Center for Magnesium Alloys, Chongqing 400045, China

Received 11 April 2020; received in revised form 3 August 2020; accepted 7 August 2020
Available online 28 September 2020

Abstract

A review of the literature confirmed that the intrinsic corrosion rate of high-purity Mg as measured by weight-loss is 0.3 mm/y in a concentrated chloride solution. Atmospheric corrosion of Mg alloys has produced corrosion rates of Mg-Al alloys an order of magnitude lower than the intrinsic corrosion rate of Mg in a concentrated chloride solution of 0.3 mm/y. The only successful strategy to produce a Mg alloy with a corrosion rate in a concentrated chloride solution substantially less than the intrinsic corrosion rate as measured by weight loss of Mg of 0.3 mm/y has been to improve the protectiveness of the corrosion product film.

Keywords: A, magnesium; B, weight loss; Polarization; EIS.

1. Introduction

Much research has been expended to understand Mg corrosion [1–6] and to produce Mg alloys with low corrosion rates, particularly in aggressive concentrated chloride solutions. Mg alloys are sought with corrosion rates as measured by weigh loss lower than the intrinsic corrosion rate of high-purity Mg of 0.3 mm/y in a concentrated chloride solution. This benchmark identifies the intrinsic corrosion rate as measured by weight loss of Mg in concentrated chloride solutions as the lowest reliable corrosion rate for Mg in these solutions [7–10]. It is of importance to understand the Mg alloy development strategies that have produced Mg alloys with low corrosion rates.

The aims of this review are:

(i) to review Mg corrosion rates,
(ii) to confirm that the intrinsic corrosion rate of high-purity Mg as measured by weight loss is 0.3 mm/y in a concentrated chloride solution,
(iii) to understand the Mg alloy development strategies that have produced Mg alloys with low corrosion rates in such solutions, and
(iv) to examine the recent claims of a new highly-corrosion-resistant Mg alloy [11,12].

To explore these aims, the recent literature of Mg corrosion was reviewed, with an emphasis on corrosion rates measured using weight loss, P_W (mm/y). Weight loss corrosion rate measurements were preferred, because there are issues with the other common methods for measuring the corrosion rate of Mg alloys [1,3,13]. The Mg corrosion rate is also evaluated (i) from the evolved hydrogen, P_H [14], (ii) by Tafel extrapolation of polarisation curves to give P_i, and (iii) from electrochemical impedance spectroscopy to give, $P_{i/EIS}$, [15].

* Corresponding author.
E-mail address: andrejs.atrens@uq.edu.au (A. Atrens).

https://doi.org/10.1016/j.jma.2020.08.002

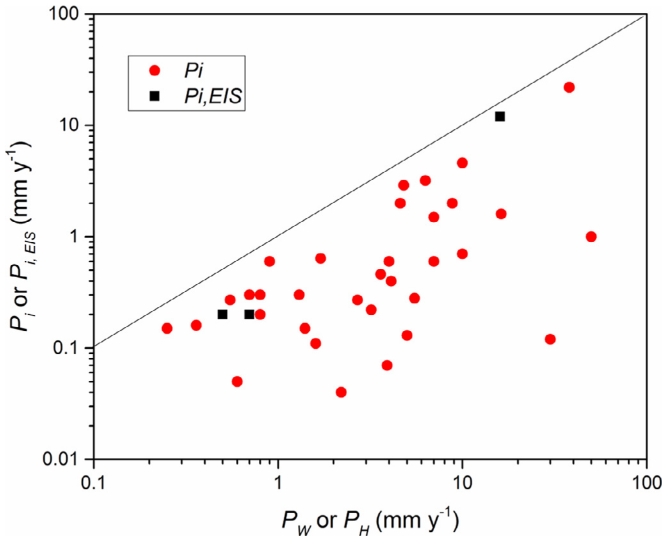

Fig. 1. Values of corrosion rate from Table 1 as measured by electrochemical techniques by Tafel extrapolation of polarisation curves, P_i or from electrochemical impedance spectra, $P_{i,EIS}$, plotted against the corrosion rate measured from the evolved hydrogen, P_H or measured by weight loss, P_W. Note that there is usually good agreement between P_H and P_W. The line drawn on the figure is a guide to the eye and shows the condition for equality of the two measurements of the corrosion rates.

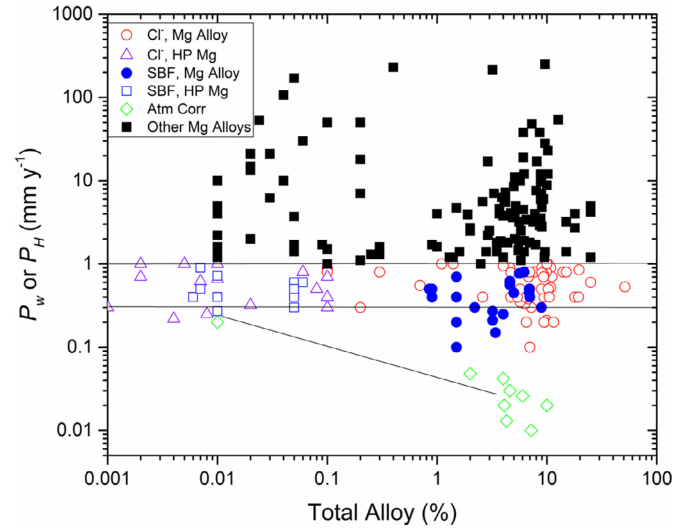

Fig. 2. Plot of the corrosion rate, P_W or P_H, against total alloying content for the Mg alloys in Table 1, with a horizontal line drawn at the intrinsic corrosion rate as measured by weight loss of Mg of 0.3 mm/y as shown by high-purity (HP) Mg and a second horizontal line drawn at a corrosion rate of 1 mm/y. These lines are drawn as a guide to the eye.

The corrosion rate of Mg measured using hydrogen evolution in a chloride solution, P_H, is typically in good agreement with the corrosion rate measured by weight loss, provided the corrosion rate is substantial [14,16,17]. This provides confidence that both techniques provide a reliable measurement of the Mg alloy steady-state corrosion rate. In contrast, experimental evidence [2,13] indicates that electrochemical measurements of the corrosion rates of Mg alloys have not provided a good measurement of the steady-state corrosion rate of Mg alloys. This is confirmed by the data in Table 1 and by Fig. 1.

The results of the review of Mg corrosion rates are presented in Table 1 and plotted in Figs. 1 and 2. In particular, Table 1 and Fig. 2 provide corrosion rates for Mg alloys in chloride solutions with an emphasis on the recent literature.

2. Electrochemical corrosion rate measurements

Fig. 1 shows the values of corrosion rate from Table 1 as measured by electrochemical techniques by Tafel extrapolation of polarisation curves, P_i, or from electrochemical impedance spectra, $P_{i,EIS}$, plotted against the corrosion rate measured from the evolved hydrogen, P_H or measured by weight loss, P_W. Note that there is usually good agreement between P_H and P_W. The plotted data do not fall on the line drawn. Thus, P_i and $P_{i,EIS}$ consistently underestimated the steady-state corrosion rates for Mg alloys in chloride solutions as measured from P_H and P_W. Fig. 1 provides reinforcement that electrochemical methods have not been reliable for the measurement of the steady-state corrosion rate of Mg alloys in concentrated chloride solutions [4,5,13].

Reasons [1,3,4] why electrochemical measurements give corrosion rates for Mg alloys less than the steady-state corrosion rates include:

(1) The corrosion rate soon after specimen immersion can be orders of magnitude smaller than the steady state corrosion rate. Electrochemical measurements are typically carried out soon after specimen immersion in the solution, before there is steady state corrosion behaviour [93,98].
(2) The evolving hydrogen (from the cathodic partial reaction) can isolate part of the specimen, so that this self-corrosion cannot be detected by any electrochemical measurement [17].

3. Mg corrosion rates

The Mg corrosion rates from Table 1 are presented in Fig. 2. Fig. 2 plots the corrosion rate, P_W and P_H, against total alloying content (TA). A horizontal line is at the intrinsic corrosion rate as measured by weight loss of Mg of 0.3 mm/y. A second horizontal line is at a corrosion rate of 1 mm/y. These lines are a guide to the eye.

Fig. 2 provides confirmation that the intrinsic corrosion rate as measured by weight loss for Mg is ~0.3 mm/y in concentrated chloride solutions as the lowest reliable corrosion rate in these solutions for high purity Mg. Research that has measured corrosion rates between 0.2 and 0.4 for HP and UHP Mg includes the following: Hanawalt, Nelson, Peloubet [7] measured $P_W = 0.3$ mm/y for alternate immersion in 3 wt% NaCl solution for 16 weeks (the specimen was dipped in the solution for 30 s, followed by 2 min in air during which the specimens did not completely dry); Cao et al. [8] measured $P_W = 0.25$ mm/y for immersion in

Table 1
Corrosion rates (CR, mm/y) for Mg alloys, with an emphasis on corrosion rates determined by weight loss, P_W. Corrosion rates from Tafel extrapolation of polarisation curves, P_i, are only quoted if these can be calculated from i_{corr} values in the paper or if i_{corr} values can be easily and accurately determined; evaluation is difficult for curved polarisation curves. P_i relates to corrosion rate evaluated by Tafel extrapolation, $P_{i,EIS}$ relates to corrosion rate evaluated from EIS [7–9,11,16–104].

Year	First Author	Alloy, condition/form	Composition, wt%	C	TA, %	Exp	M	CR, mm/y	Ref
2019	Bahmani	MgMnCa, XM11	Mg0.52Mn0.39Ca	B	0.9	1, 7 d	P_W	1.7	18
2019	Bahmani	MgMnCa, XM11	Mg0.52Mn0.39Ca	B	0.9	1, 0.5 h	P_i	0.64	18
2019	Bahmani	MgMnCaAl, AXM211	Mg0.48Mn0.42Ca2.38Al	B	3.3	1, 7 d	P_W	8.7	18
2019	Bahmani	MgMnCaAl, AXM211	Mg0.48Mn0.42Ca2.38Al	B	3.3	1, 0.5 h	P_i	1.5	18
2019	Bahmani	MgMnCaSn, TXM911	Mg0.54Mn0.49Ca9.14Sn	B	10	1, 7 d	P_W	8.8	18
2019	Bahmani	MgMnCaSn, TXM911	Mg0.54Mn0.49Ca9.14Sn	B	10	1, 0.5 h	P_i	2.0	18
2019	Bahmani	MgMnCaZn, ZXM411	Mg0.56Mn0.44Ca3.90Zn	B	4.9	1, 7 d	P_W	3.6	18
2019	Bahmani	MgMnCaZn, ZXM411	Mg0.56Mn0.44Ca3.90Zn	B	4.9	1, 0.5 h	P_i	0.46	18
2019	Cao	Pure Mg, ep	Mg0.0028 Fe	P	0.08	2, 7d	P_{AH}	0.5	19
2019	Cao	Pure Mg, ep	Mg0.0028 Fe	B	0.08	2, 7d	$P_{i,EIS}$	0.2	19
2019	Cao	Pure Mg, ep	Mg0.0028 Fe	B	0.08	3, 7d	P_{AH}	16	19
2019	Cao	Pure Mg, ep	M-0.0028 Fe	B	0.08	3, 7d	$P_{i,EIS}$	12	19
2019	Gore	Pure Mg	[Fe] < 0.001	P	0.06	4, 1 d	P_W	0.8	20
2019	Gore	Pure Mg	[Fe] < 0.001	B	0.06	4, 10 m	P_i	0.3	20
2019	Gore	Mg0.14In	[Fe] = 0.002, 0.14In	B	0.2	4, 1 d	P_W	7	20
2019	Gore	Mg0.14In	[Fe] = 0.002, 0.14In	B	0.2	4, 10 m	P_i	0.6	20
2019	Gore	Mg0.11Au	[Fe] = 0.003, 0.11Au	B	0.2	4, 1 d	P_W	50	20
2019	Gore	Mg0.11Au	[Fe] = 0.003, 0.11Au	B	0.2	4, 10 m	P_i	1.0	20
2019	Cain	AZ31B-H24	3.02Al0.99 Zn0.33Mn0.005Fe	B	4.3	5, 1 d	P_i	3.4	21
2019	Cain	Mg1Sn	1.23Sn0.02Al0.005Zn0.002Mn0.002Fe	B	1.2	5, 1 d	P_i	6.8	21
2019	Cain	Mg5Sn	5.48Sn0.03Al0.005Zn0.004Mn 0.007Fe	B	5.4	5, 1 d	P_i	4.1	21
2019	Cain	Mg10Sn	10.65Sn0.02Al 0.004Zn0.002Mn0.001Fe	B	10.6	5, 1 d	P_i	1.4	21
2019	Hu	AZ91	9.12Al0.89Zn0.23Mn	R	10.2	4, 1 d	P_W	1.0	22
2019	Hu	AZ910.5Sm	8.98Al1.12Zn0.19Mn0.48Sm	R	10.8	4, 1 d	P_W	0.9	22
2019	Hu	AZ911.0Sm	9.08Al0.96Zn0.18Mn0.92Sm	R	11.1	4, 1 d	P_W	0.7	22
2019	Kim	CP Mg	0.001Al0.001Mn0.003Y0.402Fe	B	0.4	6, 3 d	P_W	230	23
2019	Kim	Mg3Al	2.878Al0.004Mn0.003Y0.291Fe	B	3.2	6, 3 d	P_W	215	23
2019	Kim	Mg3Al0.3Mn	2.598Al0.253Mn0.003Y0.0094Fe	B	2.9	6, 3 d	P_W	17	23
2019	Kim	Mg3Al0.03Y	2.598Al0.001Mn0.033Y0.0061Fe	B	2.6	6, 3 d	P_W	5.6	23
2019	Kim	Mg3Al0.2Y	2.660Al0.001Mn0.176Y0.0051Fe	B	2.8	6, 3 d	P_W	1.4	23
2019	Kim	Mg3Al0.5Y	2.900Al0.001M 0.548Y0.0039Fe	B	3.5	6, 3 d	P_W	1.8	23
2019	Abdel-Gawad	Pure Mg	Undisclosed	B	0.01	7, 10 d	P_W	5.0	24
2019	Abdel-Gawad	Pure Mg	Undisclosed	B	0.01	7, 0.5 h	P_i	0.13	24
2019	Abdel-Gawad	Mg1Zn0.6Ca, cast	1.037Zn0.019Fe0.079V0.014Ti0.245Si0.567Ca	B	1.9	7, 10 d	P_W	3.9	24
2019	Abdel-Gawad	Mg1Zn0.6Ca, cast	1.037Zn0.019Fe0.079V0.014Ti, 0.245Si0.567Ca	B	1.9	7, 0.5 h	P_i	0.07	24
2019	Abdel-Gawad	Mg2Zn0.6Ca, cast	2.016Zn0.012Fe0.052V, 0.010Ti0.179Si0.600Ca	B	2.9	7, 10 d	P_W	2.2	24
2019	Abdel-Gawad	Mg2Zn0.6Ca, cast	2.016Zn0.012Fe0.052V0.010Ti 0.179Si0.600Ca	B	2.9	7, 0.5 h	P_i	0.04	24
2019	Abdel-Gawad	Mg2.5Zn1.5Ca, cast	2.540Zn0.013Fe0.050V0.008Ti 0.180Si1.440Ca	B	4.2	7, 10d	P_W	5.5	24
2019	Abdel-Gawad	Mg2.5Zn1.5Ca, cast	2.540Zn0.013Fe0.050V0.008Ti 0.180Si1.440Ca	B	4.2	7, 0.5 h	P_i	0.28	24
2019	Jiang	Mg4Zn, e	3.63Zn0.00Sn0.06Fe0.06Si	B	3.8	8, 7 d	P_W	1.87	25
2019	Jiang	Mg4Zn0.9Sn, e	3.56Zn0.92Sn0.04Fe 0.04Si,	Bl	4.6	8, 7 d	P_W	0.62	25
2019	Jiang	Mg4Zn1.4Sn, e	3.56Zn1.43Sn0.02Fe0.03Si,	Bl	5.0	8, 7 d	P_W	0.45	25
2019	Jiang	Mg4Zn1.9Sn, e	3.58Zn1.88Sn0.03Fe0.07Si,	Bl	5.6	8, 7 d	P_W	0.77	25
2019	Zuo	Pure Mg, e&cd	Not provided	B	0.01	9, 14 d	P_W	1.6	26
2019	Zuo	Pure Mg, e&cd	Not provided	B	0.01	10, 14 d	P_W	2.2	26
2019	Zuo	Pure Mg, e&cd	Not provided	B	0.01	11, 14 d	P_W	1.5	26
2019	Song	Mg2Zn0.5Mn1Ca1.4Ce, cast	2.00Zn0.50Mn1.02 Ca1.35 Ce	B	4 .9	12, 1 h	P_i	0.63	27
2019	Song	Mg2Zn0.5Mn1Ca1.4Ce, ECAP	2.00Zn0.50Mn1.02 Ca1.35 Ce	B	4.9	12, 1 h	P_i	0.90	27
2019	Gao	HP-Mg, e	99.99 wt%	Bl	0.01	12, 10 d	P_W	0.27	28
2019	Gao	HP-Mg, e+ts	99.99 wt%	Bl	0.01	12, 10 d	P_W	0.72	28
2019	Gao	HP-Mg, e	99.99 wt%	B	0.01	13, 8 w	P_W	0.03	28
2019	Gao	HP-Mg, e+ts	99.99 wt%	B	0.01	13, 8 w	P_W	0.03	28
2019	Dvorsky	Pure Mg, e	undisclosed	B	0.01	14, 14 d	P_W	1.2	29
2019	Dvorsky	WE43, e	Mg4Y3Nd	Bl	7.0	14, 14 d	P_W	0.4	29
2019	Dvorsky	EZ30, e	Mg3Nd0.5Zn	B	3.5	14, 14 d	P_W	1.4	29
2019	Dvorsky	WZ21, e	Mg2Y1Zn	B	3.0	14, 14 d	P_W	2.5	29
2019	Dong	Mg1.5Sr, e	Mg1.5Sr, < 0.001Fe, <0.001 Ni	Bl	1.5	12, 14 d	P_W	0.2	30
2019	Dong	Mg1.5Sr, T4 450 C for 5 h	Mg1.5Sr, < 0.001Fe, <0.001Ni	Bl	1.5	12, 14 d	P_W	0.1	30
2019	Dong	Mg1.5Sr, T4 560 C for 5 h	Mg1.5Sr, < 0.001Fe, <0.001Ni	Bl	1.5	12, 14 d	P_W	0.4	30
2019	Dong	Mg1.5Sr, T6 560 C for 5 h, 10 h at 200 C	Mg1.5Sr, < 0.001Fe, <0.001Ni	Bl	1.5	12, 14 d	P_W	0.7	30
2019	Dong	Mg1.5Sr, T6 560 C for 5 h, 40 h at 200 C	Mg1.5Sr, < 0.001Fe, <0.001 Ni	B	1.5	12, 14 d	P_W	4.7	30

(*continued on next page*)

Table 1 (*continued*)

2019	Zhao	AZ31, e	Mg3.14Al1.02Zn0.44Mn0.003Si0.0018Fe	Bl	4.6	12, 230 h	P_{AH}	0.56	31
2019	Feliu	AZ31, unspecified	Mg3.0Al1.0Zn0.2Mn	B	4.2	15, 20 C, 4 d	P_W	1.8	32
2019	Feliu	AZ31, unspecified	Mg3.0Al1.0Zn0.2Mn	B	4.2	15, 37 C, 4 d	P_W	7.2	32
2019	Grimm	Pure Mg	undisclosed	B	0.01	16, 7 d	P_W	4	33
2019	Grimm	Mg-18Al	Mg18Al0.0029Fe0.0104Si0.023Mn	B	18	16, 7 d	P_W	4	33
2019	Yan	Mg0.06Cu, cast	Mg0.057Cu-<0.005Fe-0.012Si	B	0.06	12, 7 d	P_W	30	34
2019	Yan	Mg0.06Cu, cast	Mg0.057Cu-<0.005Fe-0.012Si	B	0.06	12, 30 m	P_i	0.12	34
2019	Yan	Mg0.06Cu, sht	Mg0.057Cu-<0.005Fe-0.012Si	Bl	0.06	12, 7 d	P_W	0.6	34
2019	Yan	Mg0.06Cu, sht	Mg0.057Cu-<0.005Fe-0.012Si	B	0.06	12, 30 m	P_i	0.05	34
2019	Zhang	Mg2Nd0.2Zn	Mg2Nd0.2Cu	Bl	2.2	12, 7 d	P_W	0.3	35
2019	Johnston	HP Mg	HP Mg	Bl	0.01	17, 7 d	P_W	0.4	36
2019	Soltan	WE43B, T6	Mg3.51Y2.09Nd0.40Gd0.49Zr0.004Fe	R	6.5	1, 21 d	P_W	0.2	37
2019	Soltan	EV31A, T6	Mg2.78Nd1.35Gd0.43Zr0.003Fe	R	4.6	1, 21 d	P_W	0.9	37
2019	Soltan	Pure Mg, cast	Mg0.003Zn0.003Fe0.008Mn	B	0.01	1, 21 d	P_W	1.6	37
2019	Soltan	ZE41A, T5	Mg4.36Zn0.66Zr0.002Fe	B	5.0	1, 21 d	P_W	8.5	37
2018	Jia	Pure Mg	Mg > 99.95 wt%	Bl	0.05	18, 14 d	P_W	0.6	38
2018	Jia	Pure Mg	Mg > 99.95 wt%	Bl	0.05	18, 56 d	P_W	0.4	38
2018	Jia	Pure Mg, porous, round pores	Mg > 99.95 wt%	B	0.05	18, 14 d	P_W	3.7	38
2018	Jia	Pure Mg, porous, round pores	Mg > 99.95 wt%	B	0.05	18, 56 d	P_W	1.4	38
2018	Jia	Pure Mg, porous, irregular polyhedral	Mg > 99.95 wt%	B	0.05	18, 14 d	P_W	1.7	38
2018	Jia	Pure Mg, porous, irregular polyhedral	Mg > 99.95 wt%	Bl	0.05	18, 56 d	P_W	0.5	38
2018	Feng	Mg25Al, cast, a+b	Mg25Al	B	25	6, 6 d	P_W	4.2	39
2018	Feng	Mg25Al, sht, a+b	Mg25Al	B	25	6, 6 d	P_W	5.0	39
2018	Feng	Mg25 Al, USS, a	Mg25Al	B	25	6, 6 d	P_W	1.2	39
2018	Feng	Mg25 Al, USS + age, a + 10-100 nm b	Mg25Al	R	25	6, 6 d	P_W	0.6	39
2018	Wu	MgGdYZnZr, sht + age: surface = oxide + alpha	Mg10.2Gd5.7Y1.6Zn0.4Zr	R	18	1, 3 d	P_H	0.4	40
2018	Wu	MgGdYZnZr, sht + age: bulk = oxide + ppts	Mg10.2Gd5.7Y1.6Zn0.4Zr	B	18	1, 6 d	P_H	2.7	40
2018	Liu	Commercially pure Mg, e	Mg0.02Si0.006Fe	B	0.03	4, 24 h	P_W	21	41
2018	Liu	Mg0.2Sb, cast	Mg0.23Sn0.002Fe	B	0.2	4, 24 h	P_W	1.1	41
2018	Liu	Mg0.1Bi, cast	Mg0.13B-0.001Fe	B	0.1	4, 24 h	P_W	1.5	41
2018	Liu	Mg0.1Ge, cast	Mg0.09Ge0.003Fe	B	0.09	4, 24 h	P_W	1.7	41
2018	Liu	Mg0.3Ge, cast	Mg0.33Ge0.001Fe	R	0.3	4, 24 h	P_W	0.8	41
2018	Liu	Mg0.1Sn, cast	Mg0.11Sn0.001Fe	R	0.1	4, 24 h	P_W	0.9	41
2018	Liu	Mg0.1Pb, cast	Mg0.14Pb0.001Fe	R	0.1	4, 24 h	P_W	0.8	41
2018	Liu	CP Mg	Mg0.02Si0.06Fe	B	0.02	4, 24 h	P_W	21	42
2018	Liu	Mg1Zn, sht at 400 C, e at 180 C	Mg1Zn	B	1	4, 24 h	P_W	4.0	42
2018	Liu	Mg1Zn0.3Ge, sht at 400 C, e at 180 C	Mg1.01Zn0.27Ge	B	1.3	4, 24 h	P_W	1.2	42
2018	Liu	Mg1Zn0.5Ge, sht at 400 C, e at 180 C	Mg1.03Zn0.52Ge	B	1.6	4, 24 h	P_W	1.4	42
2018	Baek	Mg8Sn1Zn1Al, e at 280	Mg7.7Sn0.95Zn0.94Al0.009Mn0.002Fe0.002Si	B	9.6	5, 72 h	P_W	250	43
2018	Baek	Mg8Sn1Zn1Al, e at 180	Mg7.7Sn0.95Zn0.94Al0.009Mn0.002Fe0.002Si	B	9.6	5, 72 h	P_W	28	43
2018	Sadeghi	AZ31		R	4	1, 7 d	P_{AH}	0.95	44
2018	Sadeghi	AZ31+0.4Sr (or 0.8Sr)		B	4.4	1, 7 d	P_{AH}	1.8	44
2018	Liu	AZ91	Mg9.3Al0.67Zn0.25Mn0.003Fe	B	10.2	6, 1w	P_W	23	45
2018	Liu	AZ91 + fsp	Mg9.3Al0.67Zn0.25Mn0.003Fe	B	10.2	6, 1 w	P_W	12	45
2018	Zhang	Mg13Gd1.6Ag0.41Zr, sht	+0.007Fe0.0013Ni0.0011Cu	B	15.0	19, 24 h	P_W	1.4	46
2018	Zhang	Mg13Gd1.6Ag0.41Zr, sht	+0.007Fe0.0013Ni0.0011Cu	B	15.0	19, 10 m	P_i	0.15	46
2018	Zhang	Mg13Gd1.6Ag0.41Zr, aged	+0.007Fe0.0013Ni0.0011Cu	B	15.0	19, 24 h	P_W	3.2	46
2018	Zhang	Mg13Gd1.6Ag0.41Zr, aged	+0.007Fe0.0013Ni0.0011Cu	B	15.0	19, 10 m	P_i	0.22	46
2018	Zhang	Mg16Gd0.36Zr, sht	+0.007Fe0.0016Ni0.0009Cu	B	16.4	19, 72 h	P_W	0.25	46
2018	Zhang	Mg16Gd0.36Zr, sht	+0.007Fe0.0016Ni0.0009Cu	B	16.4	19, 10 m	P_i	0.15	46
2018	Zhang	Mg16Gd0.36Zr, aged	+0.007Fe0.0016Ni0.0009Cu	B	16.4	19, 72 h	P_W	0.36	46
2018	Zhang	Mg16Gd0.36Zr, aged	+0.007Fe0.0016Ni0.0009Cu	B	16.4	19, 10 m	P_i	0.16	46

(*continued on next page*)

3.5 wt% NaCl saturated with $Mg(OH)_2$ for 14 days; Yang et al. [9] measured $P_W = 0.22$ and 0.33 mm/y for immersion in 3.5 wt% NaCl solution for 2 days; Liu et al. [10] measured $P_W = 0.2$ mm/y for immersion in Hanks' solution for 3 days and 15 days (0.8 wt% NaCl, 0.14 M NaCl); Gao et al. [28] measured $P_W = 0.27$ mm/y for immersion in Hanks' solution for 10 days; Johnston [36,50] measured $P_W = 0.4$ mm/y for immersion in Hanks' solution for 1 week; Jia et al. [38] measured $P_W = 0.4$ mm/y for immersion in Dulbecco's modified eagle medium (DMEM) + 10 vol.% foetal bovine serum, 100 units/mL penicillin + 100 units/mL Streptomycin, at 37 C with 5 vol% CO_2 atmosphere for 56 days (DMEM

Table 1 (*continued*)

2018	Yang	Mg3Fe, film	Mg3Fe9Si26Mn (ppm)	P	0.004	6, 48 h	P_W	0.22	9
2018	Yang	Mg11Fe, film	Mg11Fe114Si108Mn (ppm)	P	0.02	6, 48 h	P_W	0.32	9
2018	Yang	Mg15Fe, fb	Mg15Fe16Si180Mn (ppm)	B	0.02	6, 48 h	P_W	1.98	9
2018	Yang	Mg18Fe, fb	Mg18Fe35Si176Mn (ppm)	B	0.02	6, 48 h	P_W	14.8	9
2018	Yang	Mg25Fe, fb	Mg25Fe1235Si216Mn (ppm)	B	0.04	6, 48 h	P_W	107	9
2018	Turan	AZ91, pm	99.7% purity	B	0.3	6, 24 h	P_W	1.6	47
2018	Turan	AZ91, pm	99.7% purity	B	0.3	6, 15 m	P_i	1.3	47
2018	Yan	Mg-0.1Cu, cast	Mg-0.1Cu-<0.005Fe-<0.01Si-<0.001Ni	B	0.1	20, 7 d	P_W	50	48
2018	Yan	Mg0.1Cu, sht 510 C 10 h	Mg-0.1Cu-<0.005Fe-<0.01Si-<0.001Ni	Bl	0.1	20, 7 d	P_W	1	48
2018	Li	Mg4Li, e		B	4	4, 5 d	P_W	1.8	49
2018	Li	Mg7.5Li, e		B	7.5	4, 5 d	P_W	3.2	49
2018	Li	Mg14Li, e		R	14	4, 5 d	P_W	0.8	49
2018	Johnston	HP Mg	Mg0.017Al0.001Fe0.018Ca0.008Mn	Bl	0.05	17, 7 d	P_W	0.3	50
2018	Johnston	UHP Mg	Mg0.002Zn0.004Ca-<0.001Fe	Bl	0.006	17, 7 d	P_W	0.4	50
2018	Johnston	UHP ZX00	Mg0.43Zn0.42Ca0.002Fe	Bl	0.85	17, 7 d	P_W	0.5	50
2018	Johnston	ZE41	Mg4.6Zn1.0Ce0.51La0.1Pr0.004Fe	B	6.2	17, 7 d	P_W	1.4	50
2017	Miao	Mg2.33Zn0.84Gd, e, sample A	Mg2.33Zn0.84Gd	Bl	3.2	12, 10 d	P_W	0.27	51
2017	Miao	Mg2.33Zn0.84Gd, sht + e, sample B	Mg2.33Zn0.84Gd	Bl	3.2	12, 10 d	P_W	0.21	51
2017	Xiang	Mg5Li1Al, e to 2 mm	Mg4.99Li1.07Al0.0053Fe	B	6.1	6, 14 d	P_W	38	52
2017	Xiang	Mg5Li1Al, e to 2 mm	Mg4.99Li1.07Al0.0053Fe	B	6.1	6, 20 m	P_i	22	52
2017	Xiang	Mg5Li1Al, e + 20% rd	Mg4.66Li1.03Al0.0054Fe	B	5.7	6, 14 d	P_W	10	52
2017	Xiang	Mg5Li-1Al, e + 20% rd	Mg4.66Li1.03Al0.0054Fe	B	5.7	6, 20 m	P_i	0.7	52
2017	Jia	Mg2Zn, ds	Not provided	B	2	21, 2 d	P_W	2.7	53
2017	Jia	Mg2Zn, ds	Not provided	B	2	21, 10 m	P_i	0.27	53
2017	Baek	Mg5.5Al0.7Zn0.3Mn0.5Ca	Mg5.53Al0.67Zn0.29Mn0.48Ca<0.001Y0.0021Fe	B	7.0	5, 3 d	P_W	1.8	54
2017	Baek	Mg5.5Al0.7Zn0.3Mn0.5Ca0.2Y	Mg5.53Al0.67Zn0.29Mn0.48Ca0.24Y0.0021Fe	R	7.2	5, 3 d	P_W	0.3	54
2017	Turan	CP Mg	99.7% Mg	B	0.3	6, 15 m	P_i	2.7	55
2017	Turan	Mg0.5wt.%GNP		B	0.5	6, 15 m	P_i	23	55
2017	Caralapatti	CP Mg	99.8% Mg	B	0.2	20, 200 h	P_W	18	56
2017	Caralapatti	CP Mg + HRLSP	99.8% Mg	B	0.2	20, 200 h	P_W	7	56
2017	Liu	Mg1Y	0.72Y-<0.001Fe-bal Mg	R	0.7	6, 300 h	P_H	0.55	57
2017	Liu	Mg1Y	0.72Y-<0.001Fe-bal Mg	B	0.7	6, 400 s	P_i	0.27	57
2017	Liu	Mg5Y, cast (ac)	4.72Y-<0.001Fe-bal Mg	B	4.7	6, 300 h	P_H	4.1	57
2017	Liu	Mg5Y, cast (ac)	4.72Y-<0.001Fe-bal Mg	B	4.7	6, 400 s	P_i	0.4	57
2017	Liu	Mg-5Y, ac + sht	4.72Y-<0.001Fe-bal Mg	R	4.7	6, 300 h	P_H	0.4	57
2017	Niu	Mg2.8Nd-02Zn0.4Zr	Mg2.8Nd0.2Zn0.4Zr	B	3.4	22, 1.5 y	P_{Volume}	0.15	58
2017	Choi	AZ91, cast	8.54Al0.19Mn0.74Zn0.0009Fe	B	9.5	6, 21 d	P_W	1.2	59
2017	Choi	AZ91Ti, cast	8.51Al0.26Mn1.13Zn0.0011Fe	R	9.9	6, 21 d	P_W	0.8	59
2017	Mingo	Mg9Al	12.7Al0.0155Fe0.0045Mn	B	12.7	23, 3 d	P_H	54	60
2017	Mingo	Mg9Al0.5Mn	7.3Al0.0110Fe0.4240Mn	R	7.7	23, 3 d	P_H	0.8	60
2017	Mingo	Mg9Al0.25Nd	7.0Al0.0190Fe0.0030Mn0.25Nd	B	7.3	23, 3 d	P_H	48	60
2017	Mingo	Mg9Al0.5Ca	8.7Al0.0020Fe0.0235Mn0.31Ca	B	9.0	23, 3 d	P_H	4.8	60
2017	Mingo	Mg9Al0.5Y	7.4Al0.0071Fe0.0102Mn0.45Y	B	8.0	23, 3 d	P_H	7.6	60
2017	Mingo	Mg9Al0.5Sn	8.2Al0.0077Fe0.0300Mn0.38Sn	B	8.6	23, 3 d	P_H	38	60
2016	Jayaraj	AZ31	Mg2.84Al0.98Zn0.11Mn0.002Fe	B	3.9	24, 5 d	P_W	6.3	61
2016	Jayaraj	AZ31	Mg2.84Al0.98Zn0.11Mn0.002Fe	B	3.9	24, 25 m	P_i	3.2	61
2016	Zhang	Mg6Gd0.5Zn0.4Zr, ac		Bl	6.9	25, 120 h	P_W	0.45	62
2016	Zhang	Mg6Gd0.5Zn0.4Zr, ac, sht 535 C for 12 h		Bl	6.9	25, 120 h	P_W	0.50	62
2016	Baek	AZ61	Mg5.53Al0.67Zn0.29Mn0.0021Fe	R	6.3	5, 72 h	P_W	0.33	63
2016	Esmaily	Pure Mg		G	0.01	26, 504	P_W	0.20	64
2016	Esmaily	AM20		G	2.0	26, 504	P_W	0.048	64
2016	Esmaily	AZ31		G	4.0	26, 504	P_W	0.042	64
2016	Esmaily	AM60		G	6.0	26, 504	P_W	0.026	64
2016	Esmaily	AZ91		G	10	26, 504	P_W	0.020	64
2016	Saikrishna	AZ31, e	Mg2.75Al0.91Zn0.001Fe	B	3.7	27, 3 d	P_W	4.0	65
2016	Saikrishna	AZ31, e	Mg2.75Al0.91Zn0.001Fe	B	3.7	27, 1 h	P_i	0.6	65
2016	Saikrishna	AZ31, fsp	Mg2.75Al0.91Zn0.001Fe	B	3.7	27, 3 d	P_W	4.6	65
2016	Saikrishna	AZ31, fsp	Mg2.75Al0.91Zn0.001Fe	B	3.7	27, 1 h	P_i	2.0	65
2016	Liu	Mg5Y7Gd1Nd0.5Zr	Mg7.04Gd4.531.29Nd0.49Zr						66
2016	Jafari	AZ63							67
2016	Johnston	UHP ZX00, e	Mg0.45Zn0.45Ca	Bl	0.9	17, 7 d	P_W	0.5	68
2016	Johnston	UHP ZX00, mc	Mg0.45Zn0.45Ca	Bl	0.9	17, 7 d	P_W	0.4	68
2015	Johnston	HP Mg	Mg0.007Fe	Bl	0.007	17, 166 h	P_W	0.5	69
2015	Johnston	AZ91	M8.15Al-0.64Zn0.15Mn0.005Fe	Bl	8.9	17, 166 h	P_W	0.3	69
2015	Johnston	ZE41	Mg4.59Zn1.06Ce0.006Fe0.13Y0.48La0.13Pr0.1Nd	B	6.5	17, 166 h	P_W	3.4	69
2015	Chu	WE43, sht 8 h at 525 C + WQ	Mg3.74Y2.10Nd0.45Zr0.52Gd<0.005Fe	R	6.8	1, 180 h	P_{AH}	0.70	70
2015	Chu	WE43, sht + PA: 16 at 250 C	Mg3.74Y2.10Nd0.45Zr0.52Gd<0.005Fe	R	6.8	1, 180 h	P_{AH}	0.38	70
2015	Liao	AZ80, forged (f)	Mg8.3Al0.46Zn0.22Mn-<0.1Si0.005Fe	B	9.0	6, 4 d	P_W	4.8	71
2015	Liao	AZ80, forged	Mg8.3Al0.46Zn0.22Mn<0.1Si0.005Fe	B	9.0	6, ?	P_i	2.9	71
2015	Liao	AZ80, f + aged at 170 C 10 h	Mg8.3Al0.46Zn0.22Mn<0.1Si0.005Fe	R	9.0	6, 4 d	P_W	0.9	71
2015	Liao	AZ80, f + aged at 170 C 10 h	Mg8.3Al0.46Zn0.22Mn<0.1Si0.005Fe	B	9.0	6, ?	P_i	0.6	71
2015	Yang	Pure Mg	Mg15 ppmFe16 ppmSi180 ppmMn	B	0.02	6, 48 h	P_W	1 to 3	72
2015	Yang	Pure Mg	Mg18 ppmFe35ppmSi176ppm Mn	B	0.02	6, 48 h	P_W	5.5 to 21	72

(*continued on next page*)

has a chloride concentration similar to that of Hanks' solution); and Shi and Atrens [96] measured $P_W = 0.4$ mm/y for immersion in 3.5 wt% NaCl saturated with $Mg(OH)_2$ for 3 to 20 days. Taltavull et al. [77] showed that the high-purity Mg corrosion rate is nearly independent of chloride concentration, provided that there is no micro-galvanic corrosion.

In this context it is worth repeating that the high-purity Mg that shows the intrinsic corrosion rate in chloride solutions as measured by weight loss of 0.3 mm/y contains no second phase particles and is typically in ingot form. Heat treatment of ingot Mg can cause precipitation of Fe-rich particles and much higher corrosion rates [98]. Heat treatments

Table 1 (*continued*)

2015	Yang	Pure Mg	Mg25 ppmFe123 ppmSi216ppm Mn	B	0.04	6, 48 h	P_W	87 to 120	72
2015	Gaon	AZ91D, diecast	Mg9.0Al0.68Zn0.24Mn	R	9.9	28, 14-18 d	P_W	0.21	73
2015	Gaon	MRI 153M, diecast	Mg8.0Al1.0Ca0.28Sr	R	9.4	28, 14-18 d	P_W	0.73	73
2015	Gaon	MRI 201S, diecast	Mg3.06Nd2.00Y0.41Zr	B	5.5	28, 14-18 d	P_W	1.46	73
2015	Yim	Mg-5Sn-1Zn (TZ51), e	Mg4.56Sn1.06Zn0.0021Si0.0010Fe	B	5.6	6, 3 d	P_W	3.2	74
2015	Yim	Mg-5Sn-3Zn (TZ53), e	Mg4.69Sn3.15Zn0.0021Si0.0017Fe	B	7.8	6, 3 d	P_W	4.0	74
2015	Choi	ZK60, e, sht, rolled	Mg5.23Zn0.53Zr0.019Mn<0.0002Fe	B	5.8	12, 1 d	P_W	2.5	75
2015	Choi	ZK60, e, sht, rolled, annealed 1 h	Mg5.23Zn0.53Zr0.019Mn<0.0002Fe	B	5.8	12, 1 d	P_W	1.1	75
2015	Saha	Pure Mg	ud	B	0.03	12, 16 d	P_W	6.2	76
2015	Saha	Pure Mg	ud	B	0.03	12, 5 m	P_i	1.6	76
2015	Saha	Mg0.25Zr	ud	B	0.25	12, 16 d	P_W	1.3	76
2015	Saha	Mg0.25Zr	ud	B	0.25	12, 5 m	P_i	0.3	76
2015	Saha	Mg1.0Zr	ud	B	1.0	12, 16 d	P_W	1.6	76
2015	Saha	Mg1.0Zr	ud	B	1.0	12, 5 m	P_i	0.11	76
2015	Wu	Pure Mg	ud	B	0.04	4, 24 h	P_W	10	11
2015	Wu	Pure Mg	ud	B	0.04	4, ud	P_i	4.6	11
2015	Wu	Mg11Li3Al0.2Zr0.6Y, WQAR	Mg10.95Li3.29Al0.19Zr0.59Y	R	15	4, 24 h	P_W	0.8	11
2015	Wu	Mg11Li3Al0.2Zr0.6Y, WQAR	Mg10.95Li3.29Al0.19Zr0.59Y	B	15	4, ud	P_i	0.2	11
2014	Tatavull	Pure Mg	Mg0.02Zn0.02Mn0.007Fe	B	0.05	17, 7 d	P_W	1.6	77
2014	Tatavull	Pure Mg	Mg0.02Zn0.02Mn0.007Fe	B	0.05	29, 7 d	P_W	1.6	77
2014	Tatavull	Pure Mg	Mg0.02Zn0.02Mn0.007Fe	B	0.05	30, 7 d	P_W	1.6	77
2014	Tatavull	ZE41	Mg4.7Zn0.4RE0.006Fe	B	5.1	17, 7 d	P_W	2.0	77
2014	Tatavull	ZE41	Mg4.7Zn0.4RE0.006Fe	B	5.1	29, 7 d	P_W	4.0	77
2014	Tatavull	ZE41	Mg4.7Zn0.4RE0.006Fe	B	5.1	30, 7 d	P_W	11	77
2014	Tatavull	AZ91	Mg8.2Al0.6Zn0.2Mn0.005Fe	B	8.8	17, 7 d	P_W	3.5	77
2014	Tatavull	AZ91	Mg8.2Al0.6Zn0.2Mn0.005Fe	B	8.8	29, 7 d	P_W	9.7	77
2014	Tatavull	AZ91	Mg8.2Al0.6Zn0.2Mn0.005Fe	B	8.8	30, 7 d	P_W	12	77
2014	Ha	Mg2Sn (T2)	Mg1.96Sn	B	2.0	5, 72 h	P_W	2.5	78
2014	Ha	Mg4Sn (T4)	Mg4.10Sn	B	4.1	5, 72 h	P_W	6.0	78
2014	Ha	Mg6Sn (T6)	Mg6.20Sn	B	6.2	5, 72 h	P_W	12	78
2014	Ha	Mg8Sn (T8)	Mg8.05Sn	B	8.1	5, 72 h	P_W	17	78
2014	Ha	Mg5Sn1Zn (TZ51)	Mg4.56Sn1.06Sn	B	5.6	5, 25 d	P_W	1.9	79
2014	Ha	Mg5Sn2Zn (TZ52)	Mg4.43Sn1.95Sn	R	6.4	5, 25 d	P_W	0.8	79
2014	Ha	Mg5Sn3Zn (TZ53)	Mg4.69Sn3.15Sn	B	7.9	5, 25 d	P_W	1.7	79
2014	Ha	Mg5Sn4Zn (TZ54)	Mg4.59Sn-.96Sn	B	8.6	5, 25 d	P_W	2.9	79
2014	Zhang	Mg5Gd1Zn0.6Zr (GZ51K), cast	Mg4.88Gd0.82Zn0.45Zr	Bl	6.2	25, 5 d	P_W	0.8	80
2014	Zhang	Mg5Gd1Zn0.6Zr (GZ51K), T6	Mg4.88Gd0.82Zn0.45Zr	B	6.2	25, 5 d	P_W	1.9	80
2014	Wang	AZ31, static	Undisclosed (ud)	B	4	31, 7 d	P_g	0.4	81
2014	Wang	AZ31, dynamic, FISS = 0.05 Pa	Ud	B	4	31, 7 d	P_g	1.2	81
2014	Schulter	HP Mg		P	0.01	1, 7 d	P_W	0.66	82
2014	Schulter	Mg5.7Y, SP		R	5.7	1, 2 d	P_W	0.35	82
2014	Schulter	Mg-10.8Y, SP		R	10.8	1, 2 d	P_W	0.52	82
2014	Schulter	Mg-19.6Y, SP		R	19.6	1, 2 d	P_W	0.85	82
2014	Schulter	Mg-51.3Y, SP		R	51.3	1, 2 d	P_W	0.53	82
2014	Schulter	Mg-4.7Gd, SP		R	4.7	1, 2 d	P_W	0.79	82
2014	Schulter	Mg-9.0Gd, SP		R	9.0	1, 2 d	P_W	0.78	82
2014	Schulter	Mg-19.4Gd, SP		R	19.4	1, 2 d	P_W	0.40	82
2013	Zainal Abidin	HP Mg, cast	Mg0.007Fe	Bl	0.007	17, 7-14 d	P_W	0.9	83
2013	Zainal Abidin	HP Mg, cast	Mg0.007Fe	B	0.007	32, 60 d	P_W	0.7	83
2013	Zainal Abidin	WZ21, fge	Mg1.65Y-0.85Zn0.00451Fe	Bl	2.5	17, 7-14 d	P_W	1.0	83
2013	Zainal Abidin	WZ21, fge	Mg1.65Y0.85Zn0.00451Fe	B	2.5	32, 60 d	P_W	1.0	83
2013	Zainal Abidin	AZ91, cast	Mg8.15Al0.64Zn0.0046Fe	B	8.8	17, 7-14 d	P_W	6	83
2013	Zainal Abidin	AZ91, cast	Mg8.15Al0.64Zn0.0046Fe	B	8.8	32, 60 d	P_W	0.7	83
2013	Shi	HP Mg, cast		P	0.002	1, 7 d	P_W	0.7	16
2013	Cui	AZ31 sheet	Mg3.19Al0.81Zn0.30Mn0.025Si0.006Fe	G	4.3	33, 2 y	P_W	0.013	84
2013	Kim	AZ61 ars		R	7	4 168 h	P_W	0.8	85
2013	Kim	AZ61 dr, gs = 0.002 mm		R	7	4, 168 h	P_W	0.5	85
2013	Kim	AZ61 rolled + 320 C anneal		R	7	4, 168 h	P_W	0.4	85
2013	Kim	AZ31, ars, gs = 0.020 mm		B	4	8, 2 h	P_W	3.8	86
2013	Kim	AZ31, dsr + WQ, gs = 0.0006 mm		Bl	4	8, 144 h	P_W	0.25	86
2013	Liao	AZ31B	Mg3.19Al1.05Zn0.39Mn0.003Fe	G	4 .6	34, 1 y	P_W	0.03	87
2013	Cao	UHP-Mg	ppm: 28Al, 48Zn, 1.3Mn, 1.6Fe, 0.34Cu, 1.4Si	P	0.008	1, 14 d	P_W	0.25	8
2013	Cao	HP Mg	ppm: 1 Fe, 20Si, 8 Mn	P	0.007	1, 7 d	P_W	0.62	17
2013	Cao	Mg1Mn, sht & WQ	1.1%Mn	R	1.1	1, 7 d	P_W	1.0	17
2012	Peng	Mg1.2RE0.2Zr	nd	R	1.4	21, nd	P_W	1.0	88
2012	Peng	Mg1.2RE0.2Zn0.2Zr	nd	B	1.4	21, nd	P_W	1.2	88
2012	Liao	AZ31B, e	Mg3.19Al1.05Zn0.39Mn0.003Fe	R	4.6	4, 90 d	P_W	0.6	89
2012	Liao	AM60, e	Mg6.07Al0.02Zn0.30Mn0.001Fe	R	6.4	4, 90 d	P_W	0.4	89
2012	Argade	Mg4Y3Nd, hr, gs 0.07 mm	nd	R	7	6, 21 d	P_W	0.4	90
2012	Argade	Mg4Y3Nd, FSP, gs 0.0017 mm	nd	R	7	6, 21 d	P_W	0.1	90
2012	Song	MgxZn							91

(*continued on next page*)

are associated with processing steps such as extrusion to form rod material. For such heat-treated material, the Fe tolerance limit may be less than ~2 ppm [98].

Fig. 2 presents data (as green diamonds) for the corrosion rate for atmospheric corrosion or simulated atmospheric corrosion of HP Mg and Mg-Al alloys. There was a significant decrease in the atmospheric corrosion rate with increasing Al content, attributed to a more protective surface film, with increasing Al content. This indicates that stable protective films form during atmospheric corrosion, whereas the films that form on similar Mg alloys during solution exposure are not protective. A key factor seems to be the dry-

Table 1 (*continued*)

2012	Arrabal	AM50	Mg4.9Al0.26Mn	B	5.2	6, 10 d	P_W	5	92
2012	Arrabal	AM500.8Nd	Mg4.4Al0.21Mn0.8Nd	R	5.4	6, 10 d	P_W	0.4	92
2012	Arrabal	AM501.5Nd	Mg4.0Al0.24Mn1.5Nd	R	5.7	6, 10 d	P_W	0.5	92
2012	Arrabal	AZ91D	Mg8.9Al0.52Zn0.19Mn	B	9.6	6, 10 d	P_W	1.4	92
2012	Arrabal	AZ91D0.7Nd	Mg8.1Al0.52Zn0.13Mn0.7Nd	R	9.5	6, 10 d	P_W	0.2	92
2012	Arrabal	AZ91D1.4Nd	Mg8.1Al0.52Zn0.16Mn1.4Nd	R	10.2	6, 10 d	P_W	0.5	92
2012	Liu	MgxY (x = 2-7)							93
2012	Qiao	HP Mg	Mg0.1Al0.017Mn0.002Fe	P	0.1	1, 7 d	P_W	0.7	94
2012	Qiao	HP Mg	Mg0.1Al0.017Mn0.002Fe	B	0.1	1, 7 d	P_i	0.3	94
2012	Qiao	HP Mg	Mg0.1Al0.017Mn0.002Fe	B	0.1	1, 7 d	$P_{i/EIS}$	0.2	94
2011	Feliu	AZ31	Mg3.1Al0.73Zn0.25Mn0.005Fe	G	4.1	35, 60 d	P_W	0.02	95
2011	Feliu	AZ61	Mg6.2Al0.74Zn0.23Mn0.004Fe	G	7.2	35, 60 d	P_W	0.01	95
2011	Shi	HP Mg, cast	Mg0.1Al0.002Fe0.017Zn	P	0.1	1, 3 to 20 d	P_W	0.4	96
2011	Zhang	AZ91, cast	Mg8.51Al0.64Zn0.22Mn	R	9.4	6, 12 h	P_W	0.2	97
2011	Zhang	AZ91, e	Mg8.51Al0.64Zn0.22Mn	R	9.4	6, 12 h	P_W	0.4	97
2009	Liu	LP Mg, GpM	Mg0.0280Fe0.017Mn	B	0.05	28, 8 h	P_H	170	98
2009	Liu	HP Mg, cast	Mg0.0045Fe0.0080Mn	P	0.01	28, 224 h	P_H	1	98
2009	Liu	HP Mg, sht 1 d at 550 C	Mg0.0045Fe0.0080Mn	B	0.01	28, 224 h	P_H	10	98
2008	Chang	AZ91D	Mg9Al1Zn	R	10	36, 3 d	P_W	1.0	99
2008	Chang	NZ30K	Mg3Nd0.2Zn0.4Zr	R	2.6	36, 3 d	P_W	0.4	99
2008	Zhao	HP Mg, cast	Mg0.0045Fe	P	0.005	37, 2 d	P_W	1	100
2008	Ben-Haroush	AZ80, cast	Mg8.33Al0.12Mn0.41Zn0.006Si0.0025Fe	R	8.9	1, 3 d	P_W	0.5	101
2008	Ben-Haroush	AZ80, cast + e at 250 C	Mg8.33Al0.12Mn0.41Zn0.006Si0.0025Fe	B	8.9	1, 3 d	P_W	7	101
2008	Ben-Haroush	AZ80, cast + e at 300 C	Mg8.33Al0.12Mn0.41Zn0.006Si0.0025Fe	B	8.9	1, 3 d	P_W	11	101
2008	Ben-Haroush	AZ80, cast + e at 350 C	Mg8.33Al0.12Mn0.41Zn0.006Si0.0025Fe	B	8.9	1, 3 d	P_W	10	101
2007	Rzychon	EV31A	Mg2.7Nd4.2R-1.2Gd0.4Zn0.5Zr	B	9	6, 7 d	P_W	2.8	102
2007	Rzychon	WE43	Mg4.0Y2.4Nd3.3RE0.6Zr	R	10.3	6, 7 d	P_W	0.5	102
2005	Wu	AZ91D	Mg9Al0.5Zn	B	9.5	36, 3 d	P_W	9	103
2005	Wu	AZ91D-2Ca	Mg9Al0.5Zn2Ca	R	11.5	36, 3 d	P_W	0.2	103
2005	Wu	AZ91D1RE	Mg9Al0.5Zn1RE	R	10.5	36, 3 d	P_W	0.4	103
2005	Wu	AZ91D1RE1Ca	Mg9Al0.5Zn1RE1Ca	R	11.5	36, 3 d	P_W	0.2	103
1999	Song	LP Mg	Mg0.024Fe	B	0.024	38, 1d	P_W	53	104
1999	Song	AZ91D, dcx	Mg8.4Al0.73Zn0.012Fe0.18Mn	B	9.3	38, 1 d	P_W	6	104
1999	Song	HP Mg	Mg0.0017Fe	P	0.002	38, 1 d	P_W	1	104
1999	Song	AZ91D, dcs= die cast-surface	Mg8.4Al0.73Zn0.012Fe0.18Mn	R	9.3	38, 1 d	P_W	0.7	104
1942	Hanawalt	UHP Mg	Mg0.001Fe	R	0.001	39, 112 d	P_W	0.3	7
1942	Hanawalt	UHP Mg	Mg0.001Ni0.2Mn	R	0.2	39, 112 d	P_W	0.3	7
1942	Hanawalt	UHP Mg	Mg0.1Cu	R	0.1	39, 112 d	P_W	0.3	7

In "Alloy, condition/form", ep = extruded plate; ***e*** = extruded; e&cd = extruded and cold drawn; *e*+ts = extruded plus applied tensile stress; sht = solution heat treated; *a*+*b* = alpha + beta; USS = ultra-high-pressure solid solution; *a* = alpha; CP = commercially pure; fsp = friction stir processing; fb = film breakdown; pm = powder metallurgy production; rd = rolling reduction; ds = directional solidification; mc = mechanically cleaned; SP = sputter deposited; fge = fine grained extrusion; ars = as received sheet; dr = differential rolling, gs = grain size; hr = hot rolled; GpM = Goodfellow pure Mg;, dcx = die cast-section; dcs= die cast-surface.

CR = corrosion rate, mm/y. TA is total alloying content, wt%. Immersion time is in m (minute), h (hour) or d (day); ? indicates undisclosed. M is method of corrosion rate measurement. Exp represents exposure condition and time: 1 = 3.5 wt% NaCl saturated with $Mg(OH)_2$; 2 = 0.4 M Na_2SO_4; 3 = 0.4 M $(NH_4)_2SO_4$; 4 = 0.1 M NaCl; 5 = 0.6 M NaCl; 6 = 3.5% NaCl; 7 = SBF + TRIS for pH control (pH control was not effective); 8 = PBS; 9 = mSBF + HEPES; 10 = Urine; 11 = Bile; 12 = Hanks' solution, 37C, no buffer; 13 = In vivo, subcutaneous, rats; 14 = SBF, details undisclosed; 15 = Ringer's solution; 16 = 5 wt.% NaCl saturated with $Mg(OH)_2$; 17 = Nor's solution: Hanks' solution, pH control by bubbling CO_2 through solution, 37 C; 18 = Dulbecco's modified eagle medium (DMEM) + 10 vol.% foetal bovine serum, 100 units/mL penicillin + 100 units/mL Streptomycin, at 37 C with 5 vol% CO_2 atmosphere; 19 = 0.01 M NaCl; 20 = Hanks' solution, no buffer, room temperature; 21 = 0.9 wt. NaCl; 22 = In vivo, New Zealand Rabits; 23 = 0.5 wt.% NaCl; 24 = 1 wt% NaCl; 25 = SBF, 37 C; 26 = Simulated atmospheric corrosion: 95%RH, 400 ppm CO_2, 70 $\mu g/cm^2$ NaCl, 504 h, 22 C; 27 = 0.9% NaCl, 37 C; 28 = 3% NaCl; 29 Nor's solution with chloride concentration adjusted to 0.3 M NaCl; 30 Nor's solution with chloride concentration adjusted to 1.0 M NaCl; 31 = Dulbeco's modified Eagle's medium (DMEM) with 10% foetal bovine serum (FBS), 1% penicillin, pH adjusted to 7.4 at start of test, P_g determined from depth of corrosion products; 32 = Sub-cutaneous in male Wistar rats; 33 = Tropical marine atmosphere, XiSha island China; 34 = Atmospheric corrosion, marine (Shimizsu City, Japan) and urban (Osaka City, Japan); 35 = Continuous condensation chamber, 100% RH, specimen slightly colder so condensation occurs on the specimen; 36 = 5% NaCl; 37 = 1 N NaCl; 38 = 1 N NaCl pH 11; 39 Alternate immersion in 3% NaCl.

The colour (C) in Table 1 and Fig. 2 is as follows: purple (P) indicates high-purity Mg in concentrated chloride solutions; red (R) indicates Mg alloys in concentrated chloride solutions; blue (Bl) indicates corrosion in synthetic body fluids (blue squares for HP Mg alloys with a total alloying less than 0.1 wt%, blue full circles for Mg alloys); green (G) diamonds for atmospheric corrosion or simulated atmospheric corrosion; black (B) for other Mg alloys, for which electrochemical measurements values are in blue.

ing which occurs periodically during atmospheric exposure [105,106].

Fig. 2 shows that Mg alloys typically have corrosion rates in chloride solutions greater than the intrinsic corrosion rate of Mg of 0.3 mm/y, and most corrosion rates are above 1 mm/y, as shown by the full black squares in 2. Mg is the most active engineering metal with a high tendency to corrode, and little protection is provided by corrosion product films. Mg alloys typically have phases in addition to the alpha-Mg matrix. These second phases typically accelerate corrosion by micro-galvanic interaction with the matrix, so that the typical corrosion rates in chloride solutions are greater than 1 mm/y [1–5]. With the two exceptions presented below, despite claims to the contrary, there is no Mg alloy with a corrosion rate (measured by weight loss) in a concentrated chloride solution much lower than the intrinsic Mg corrosion rate of 0.3 mm/y in a concentrated chloride solution. This is evidenced by the data presented in Table 1 and Fig. 2.

The two exceptions of Mg alloys with a corrosion rate (measured by weight loss) in a chloride solution much lower than the intrinsic Mg corrosion rate of 0.3 mm/y are the Mg alloys with weight loss corrosion rates of 0.1 mm/y: (i) Mg-1.5Sr [30], and (ii) Mg-4Y-3Nd [90]. Argade, Panigrahi and Mishra [90] reported a corrosion rate of 0.1 mm/y for a Mg-4Y-3Nd alloy with a grain size of 0.0017 mm, see Table 1 and Fig. 1. This corrosion rate below the intrinsic Mg corrosion rate seems to have been produced by a more protective surface film. In addition, this research provided clear evidence of a significant decrease of corrosion rate caused by a decrease in grain size, which could be related to the increased impurity tolerance after grain refinement [107]. Similarly, the Mg-1.5Sr of Dong et al. [30] had a corrosion rate below the intrinsic Mg corrosion rate. Thus, the only successful Mg alloy development strategy relates to Mg alloys that have produced more protective surface films on immersion in solution.

This Mg alloy development strategy was suggested by Song and Atrens [4] in 2003; a stainless Mg alloy might be possible if a Mg alloy could be produced that spontaneously produces a much more protective corrosion product film. This suggestion was based on the analogy with stainless steels which can be considered as Fe-Cr alloys, and which typically spontaneously form a passive surface oxide (approximately Cr_2O_3) for a Cr content greater than 10.5 wt.%.

Fig. 2 does also indicate that there are a significant number of alloys [9,16,17,20,39,41,49,54,82,90,94,96,104], including commercial alloys or modified commercial alloys [22,37,59,63,79,85,89,92,97,99,101–103], with corrosion rates in chloride solutions comparable to the intrinsic corrosion rate of Mg of 0.3 mm/y in a concentrated chloride solution [7–9]. These Mg alloys are plotted in Fig. 2 as red circles for corrosion in chloride solutions, and as full blue circles for corrosion in various synthetic body fluids, (SBFs).

Thus, it is demonstrably not accurate or reasonable to claim that an alloy with a corrosion rate as measured by weight loss above 0.3 mm/y in a concentrated chloride solution has a corrosion rate much lower than any existing Mg alloy [11]. The lowest corrosion rate of the Mg-Li alloy described by Xu et al. [11] was $P_W = 0.8$ mm/y (see Table 1) and was substantially above the intrinsic corrosion rate as measured by weight loss of Mg of 0.3 mm/y. This Mg alloy was claimed to have a corrosion rate much lower than any existing Mg alloy [11,12]. For example: “Here we design an ultralow density (1.4 g cm^{-3}) Mg–Li-based alloy that is strong, ductile, and more corrosion resistant than Mg-based alloys reported so far” [11]; “Ferry and colleagues [11] describe the development of a new alloy with a combined improvement in strength, ductility, and corrosion resistance, compared with other Mg alloys” [12], and “Emergence of “stainless” Mg alloy” as a landmark in the scientific and technical development of magnesium corrosion research [6]. These claims were not supported by the experimental evidence of Table 1 and Fig. 2.

It was also suggested that low corrosion rates in chloride solutions could be produced by decreasing the cathodic partial reaction of hydrogen evolution [41,42,108,109]. In each case $P_W \geq 0.8$ mm/y. This corrosion rate was substantially above the intrinsic corrosion rate as measured by weight loss of Mg of 0.3 mm/y, and so this approach has not produced a Mg alloy with a corrosion rate substantially less than the intrinsic corrosion rate as measured by weight loss of Mg of 0.3 mm/y.

4. Conclusions

1. A review of the literature confirmed that the intrinsic corrosion rate as measured by weight loss of high-purity Mg is 0.3 mm/y in a concentrated chloride solution.
2. Atmospheric corrosion of Mg alloys has produced corrosion rates of Mg-Al alloys an order of magnitude lower than the intrinsic corrosion rate of Mg in a concentrated chloride solution of 0.3 mm/y,
3. Two Mg alloys, (namely Mg-1.5Sr, and Mg-4Y-3Nd) were identified with corrosion rates as measured by weight loss less than the intrinsic corrosion rate of high-purity Mg of 0.3 mm/y in a concentrated chloride solution,
4. The only successful strategy to produce a Mg alloy with a corrosion rate as measured by weight loss substantially less than the intrinsic corrosion rate as measured by weight loss of Mg of 0.3 mm/y has been to improve the protectiveness of the corrosion product film,
5. Corrosion rates for Mg alloys measured by electrochemical methods are typically lower than the steady-state corrosion rates measured by weight loss, often by orders of magnitude,
6. The recent claims that new Mg alloys have been produced that are more corrosion resistant than Mg-based alloys reported so far are not supported by the literature.

Acknowledgements

This work was supported by the Australian Research Council Discovery Project DP170102557.

Data availability

The data required to reproduce these findings are from the published literature and are available within the paper

References

[1] A. Atrens, S. Johnston, Z. Shi, M.S. Dargusch, Scr Mater 154 (2018) 92.
[2] A. Atrens, G.-L. Song, M. Liu, Z. Shi, F. Cao, M.S. Dargusch, Adv Eng Mater 17 (2015) 400–453.
[3] A. Atrens, G.L. Song, F. Cao, Z. Shi, P.K. Bowen, J Magnes Alloys 1 (2013) 177–200.
[4] G. Song, A. Atrens, Adv Eng Mater 5 (2003) 837–858.
[5] G. Song, A. Atrens, Adv Eng Mater 1 (1999) 11–33.
[6] M. Esmaily, et al., Prog Mater Sci 89 (2017) 92.
[7] J.D. Hanawalt, C.E. Nelson, J.A. Peloubet, Trans Am Inst Min Metall Eng 147 (1942) 273.
[8] F. Cao, Z. Shi, J. Hofstetter, P.J. Uggowitzer, G. Song, M. Liu, A. Atrens, Corros Sci 75 (2013) 78–99.
[9] L. Yang, G. Liu, L. Ma, E. Zhang, X. Zhou, G. Thompson, Corros Sci 139 (2018) 421–429.
[10] J. Liu, et al., Acta Biomater 102 (2020) 508–528.
[11] W. Xu, N. Birbilis, G. Sha, Y. Wang, J.E. Daniels, Y. Xiao, M. Ferry, Nat Mater 14 (2015) 1229–1235.
[12] G.S. Frankel, Nat Mater 14 (2015) 1189.
[13] Z. Shi, M. Liu, A. Atrens, Corros Sci 52 (2010) 579–588.
[14] G.L. Song, A. Atrens, D. St.John, Magnes Technol (2001) 255–262.
[15] Z. Shi, F. Cao, G.-L. Song, A. Atrens, Corros Sci 88 (2014) 434–443.
[16] Z. Shi, F. Cao, G.L. Song, M. Liu, A. Atrens, Corros Sci 76 (2013) 98–118.
[17] F. Cao, Z. Shi, G.L. Song, M. Liu, A. Atrens, Corros Sci 76 (2013) 60–97.
[18] A. Bahmani, S. Arthanari, K.W. Shin, J Magnes Alloys 7 (2019) 38–46.
[19] F. Cao, C. Zhao, G.L. Song, D. Zheng, Corros Sci 150 (2019) 161–174.
[20] P. Gore, T.W. Cain, J. Laird, J.R. Scully, N. Birbilis, V.S. Raja, Corros Sci 151 (2019) 206–218.
[21] T.W. Cain, C.F. Glover, J.R. Scully, Electrochim. Acta 297 (2019) 564–575.
[22] Z. Hu, R.L. Liu, S.K. Kary, X. Li, H. Yan, N. Birbilis, Corros Sci 149 (2019) 144–152.
[23] J.I. Kim, H.N. Nguyen, B.S. You, Y.M. Kim, Scr Mater 162 (2019) 355–360.
[24] S.A. Abdel-Gawad, M.A. Shoeib, Surf Interfaces 14 (2019) 108–116.
[25] W. Jiang, J. Wang, W. Zhao, Q. Liu, D. Jiang, S. Guo, J Magnes Alloys 7 (2019) 15–26.
[26] M. Zuo, W. Wang, H. Wu, L. Yang, J. Yan, J. Ni, S. Zhang, Y. Song, J. Wang, X. Zhang, Mater Lett 240 (2019) 279–283.
[27] D. Song, C. Li, N. Liang, F. Yang, J. Jiang, J. Sun, G. Wu, A. Ma, X. Ma, Mater Des 166 (2019) 107621.
[28] Y. Gao, L. Wang, L. Li, X. Gu, K. Zhang, J. Xie, Y. Fan, Acta Biomater 83 (2019) 477–486.
[29] D. Dvorsky, J. Kubaswk, I. Vonavkova, D. Vojtech, Mater Sci Technol 35 (2019) 520–529.
[30] J.H. Dong, L.L. Tan, Y.B. Ren, K. Yang, Acta Metall Sin (English Lett) 32 (2019) 305–320.
[31] J. Zhao, X. Chen, S. Li, R. Zheng, F. Zhang, Z. Wang, J Colloids Interface Sci 547 (2019) 309–317.
[32] S. Feliu Jr, L. Veleva, F. Garcia-Galvan, Metals (Basel) 9 (1–17) (2019) 591.
[33] M. Grimm, A. Lohmuller, R.F. Singer, S. Virtanen, Corros Sci 155 (2019) 195–208.
[34] X. Yan, M.C. Zhao, Y. Yang, L. Tan, Y. Zhao, D. Yin, K. Yang, A. Atrens, Corros Sci 156 (2019) 125–138.
[35] W. Zhang, L. Tan, D. Ni, J. Chen, Y. Zhao, L. Liu, C. Shui, K. Yang, A. Atrens, M.C. Zhao, J Mater Sci Technol 35 (2019) 777–783.
[36] S. Johnston, Z. Shi, J. Venezuela, C. Wen, M.S. Dargusch, A. Atrens, JOM 71 (4) (2019) 1406–1413.
[37] A. Soltan, M.D. Dargusch, Z. Shi, D. Gerrard, A. Atrens, Mater Corros 70 (2019) 1527–1552, doi:10.1002/maco.201910845.
[38] G. Jia, C. Chen, J. Zhang, Y. Wang, R. Yue, B.J.C. Luthringer-Feyerabend, R. Willumeit-Roemer, H. Zhang, M. Xiong, H. Huang, G. Yuan, F. Feyerabend, Corros Sci 144 (2018) 301–312.
[39] J. Feng, H. Li, K. Deng, C. Fernandez, Q. Zhang, Q. Peng, Corros Sci 143 (2018) 229–239.
[40] L. Wu, H. Li, Corros Sci 142 (2018) 238–248.
[41] R.L. Liu, J.R. Scully, G. Williams, N. Birbilis, Electrochim. Acta 260 (2018) 184–195.
[42] R.L. Liu, Z.R. Zeng, J.R. Scully, G. Williams, N. Birbilis, Corros Sci 140 (2018) 18–29.
[43] S.M. Baek, J.S. Kang, J.C. Kim, B. Kim, S.S. Park, H.J. Shin, Corros Sci 141 (2018) 203–210.
[44] A. Sadeghi, E. Hasanpur, A. Bahmani, K.S. Shin, Corros Sci 141 (2018) 117–126.
[45] Q. Liu, Q. Ma, G. Chen, X. Gao, S. Zhang, J. Pan, G. Zhang, Q. Shi, Corros Sci 138 (2018) 284–296.
[46] Y. Zhang, P. Gore, W. Rong, Y. Wu, Y. Yan, R. Zhang, L. Peng, J. Nie, N. Birbilis, Corros Sci 136 (2018) 106–118.
[47] M.E. Turan, Y. Sun, F. Aydin, H. Zengin, Y. Turen, H. Ahlatci, Mater Chem Phys 218 (2018) 182–188.
[48] X. Yan, P. Wan, L. Tan, M. Zhao, L. Qin, K. Yang, Mater Sci Eng C 93 (2018) 565–581.
[49] C.Q. Li, D.K. Xu, X.B. Chen, B.J. Wang, R.Z. Wu, E.H. Han, N. Birbilis, Electrochim Acta 260 (2018) 55–64.
[50] S. Johnston, et al., J Biomed Mater Res B: Appl Biomater 106B (2018) 1907–1917.
[51] H. Miao, H. Huang, Y. Shi, H. Zhang, J. Pei, G. Yuan, Corros Sci 122 (2017) 90–99.
[52] Q. Xiang, B. Jiang, Y. Zhang, X. Chen, J. Song, J. Xu, L. Fang, F. Pan, Corros Sci 119 (2017) 14–22.
[53] H. Jia, X. Feng, Y. Yang, Corros Sci 120 (2017) 75–81.
[54] S.M. Baek, J.S. Kang, H.J. Shin, C.D. Yim, B.S. You, H.Y. Ha, S.S. Park, Corros Sci 118 (2017) 227–232.
[55] M.E. Turan, Y. Sun, Y. Akgul, Y. Turen, H. Achlatci, J Alloys Compd 724 (2017) 14–23.
[56] V.K. Caralapatti, S. Narayanswamy, Opt Laser Technol 88 (2017) 75–84.
[57] X. Liu, D. Shan, Y. Song, E.-H. Han, J Magnes Alloys 5 (2017) 26–34.
[58] J. Niu, M. Xiong, X. Guan, J. Zhang, H. Huang, J. Pei, G. Yuan, Corros Sci 113 (2016) 183–187.
[59] H.Y. Choi, W.J. Kim, J Alloys Compd 696 (2017) 736–745.
[60] B. Mingo, R. Arrabal, M. Mohedano, C.L. Mendis, R. del Olmo, E. Matykin, N. Hort, Mater Des 130 (2017) 48–58.
[61] J. Jayaraj, S.A. Raj, A. Srinivasan, S. Ananthakumar, Corros Sci 113 (2016) 104–115.
[62] X. Zhang, Z. Ba, Z. Wang, Y. Xue, Corros Sci 105 (2016) 68–77.
[63] S. Baek, H.J. Kim, H.Y. Jeong, S. Sohn, H.J. Shin, K. Choi, K. Lee, J.G. Lee, G.D. Yim, B.S. You, H.Y. Ha, S.S. Park, Corros Sci 112 (2016) 44–53.
[64] M. Esmaily, D.B. Blucher, J.E. Svensson, M. Halvarsson, L.G. Johansson, Scr Mater 115 (2016) 91–95.
[65] N. Saikrishna, G.P.K. Reddy, B. Munirathinam, B.R. Sunil, J Magnes Alloys 4 (2016) 68–76.
[66] J. Liu, Y. Song, J. Chen, P. Chen, D. Shan, E.H. Han, Electrochim Acta 189 (2016) 190–195.
[67] H. Jafari, P. Amiryavari, Mater Sci Eng A 654 (2016) 161–168.
[68] S. Johnston, Z. Shi, M.S. Dargusch, Corros Sci 108 (2016) 66–75.
[69] S. Johnston, Z. Shi, A. Atrens, Corros Sci 101 (2015) 182–192.
[70] P.W. Chu, E.A. Marquis, Corros Sci 101 (2015) 94–104.
[71] H. Liao, X. Zhou, H. Li, M. Deng, X. Liang, R. Liu, Trans Nonferrous Met Soc China 25 (2015) 3921–3927.

[72] L. Yang, X. Zhou, S. Liang, R. Schmid-Fetzer, Z. Fan, G. Scamans, J. Robson, G. Thompson, J Alloys Compd 619 (2015) 396–400.
[73] O. Gaon, G. Dror, O. Davidi, A. Lugovskoy, Corros Sci 93 (2015) 167–171.
[74] C.D. Yim, J. Yang, S.K. Woo, H.Y. VHa, B.S. You, Corros Sci 90 (2015) 597–605.
[75] H.Y. Choi, W.J. Kim, J Mech Behav Biomed Mater 51 (2015) 291–301.
[76] P. Saha, M. Roy, M.K. Data, B. Lee, P.N. Kumta, Mater Sci Eng C 57 (2015) 294–303.
[77] C. Taltavull, Z. Shi, B. Torres, J. Rams, A. Atrens, J Mater Sci: Mater Med 25 (2014) 329–345.
[78] H.Y. Ha, J.Y. Kang, S.G. Kim, B. Kim, S.S. Park, C.D. Yim, B.S. You, Corros Sci 82 (2014) 369–379.
[79] H.Y. Ha, J.Y. BKang, C.D. Yim, J. Yang, B.S. You, Corros Sci 89 (2014) 275–285.
[80] X. Zhang, Z. Ba, Q. Wang, Y. Wu, Z. Wang, Q. Wang, Corros Sci 88 (2014) 1–5.
[81] J. Wang, V. Giridharan, V. Shanov, Z. Xu, B. Collins, L. White, Y. Jang, J. Sankar, N. Huang, Y. Yun, Acta Biomater 10 (2014) 5213–5223.
[82] K. Schlüter, Z. Shi, C. Zamponi, F. Cao, E. Quandt, A. Atrens, Corros Sci 78 (2014) 43–54.
[83] N.I. Zainal Abidin, B. Rolfe, H. Owen, J. Malisano, D. Martin, J. Hofstetter, P.J. Uggowitzer, A. Atrens, Corros Sci 75 (2013) 354–366.
[84] Z. Cui, X. Li, K. Xiao, C. Dong, Corros Sci 76 (2013) 243–256.
[85] H.S. Kim, W.J. Kim, Corros Sci 75 (2013) 228–238.
[86] H.S. Kim, G.H. Kim, H. Kim, W.J. Kim, Corros Sci 74 (2013) 139–148.
[87] J. Liao, M. Hotta, S. Motoda, T. Shinohara, Corros Sci 71 (2013) 53–61.
[88] Q. Peng, Y. Huang, K.U. Kainer, N. Hort, Adv Eng Mater 14 (2012) 178–184.
[89] J. Liao, M. Hotta, N. Yamamoto, Corros Sci 61 (2012) 208–214.
[90] G.R. Argade, S.K. Panigrahi, R.S. Mishra, Corros Sci 58 (2012) 145–151.
[91] Y. Song, E.H. Han, D. Shah, C.D. Yim, B.S. You, Corros Sci 65 (2012) 322–330.
[92] R. Arrabal, Effect of Nd on the corrosion behaviour of AM50 and AZ91D magnesium alloys in 3.5wt.% NaCl solution, Corros Sci 55 (2012) 301–312.
[93] M. Liu, P. Schmutz, P.J. Uggowitzer, G. Song, A. Atrens, Corros Sci 52 (2010) 3687–3701.
[94] Z. Qiao, Z. Shi, N. Hort, N. Zainal Abidin, A. Atrens, Corros Sci 61 (2012) 185–207.
[95] S. Feliu Jr, C. Maffiotte, J.C. Galvan, V. Barranco, Corros Sci 53 (2011) 1865–1872.
[96] Z. Shi, A. Atrens, Corros Sci 53 (2011) 226–246.
[97] T. Zhang, Y. Shao, G. Meng, Z. Cui, F. Wang, Corros Sci 53 (2011) 1960–1968.
[98] M. Liu, P.J. Uggowitzer, A.V. Nagasekhar, P. Schmutz, M. Easton, G. Song, A. Atrens, Corros Sci 51 (2009) 602–619.
[99] J.W. Chang, J Appl Electrochem 38 (2008) 207–214.
[100] M.C. Zhao, M. Liu, G. Song, A. Atrens, Corros Sci 50 (2008) 1939–1953.
[101] M. Ben-Haroush, et al., Corros Sci 50 (2008) 1766–1778.
[102] T. Rzychon, J. Michalska, A. Kielbus, J Achiev Mater Manuf Eng 21 (2007) 51–54.
[103] G. Wu, et al., Mater Sci Eng A 408 (2005) 255–263.
[104] G.L. Song, A. Atrens, M. Dargusch, Corros Sci 41 (1999) 249–273.
[105] M.C. Zhao, P. Schmutz, S. Brunner, M. Liu, G. Song, A. Atrens, Corros Sci 51 (2009) 1277–1292.
[106] G.L. Song, S. Hapugoda, D. StJohn, Corros Sci 49 (2007) 1245–1265.
[107] G.L. Song, Z. Xu, Corros Sci 54 (2012) 97–105.
[108] N. Birbilis, G. Williams, K. Gusieva, A. Samaniego, M.A. Gibson, H.N. McMurray, Electrochem Commun 34 (2013) 295–298.
[109] D. Eaves, G. Williams, H.N. McMurray, Electrochim Acta 79 (2012) 1–7.